Orthorhombic full-waveform inversion for wide-azimuth data imaging

Yi Xie[1], Bin Zhou[2], Joe Zhou[1], Jiangtao Hu[1], Lei Xu[1], Xiaodong Wu[1], Nina Lin[1], and Zhiliang Wang[2]*
[1]CGG; [2]CNOOC Ltd-Tianjin

Summary

The presence of orthorhombic anisotropy poses significant challenges in multi-azimuth (MAZ) or wide-azimuth (WAZ) data imaging. Orthorhombic anisotropy causes seismic velocity to vary with azimuthal direction as well as with polar direction. The polar direction dependency causes well misties and higher order moveout. On the other hand, the azimuthal dependency can cause noticeable moveout fluctuations between different acquisition directions and hence prevent constructive summation of WAZ images, especially when imaging faults. In this paper we develop an orthorhombic full-waveform inversion (FWI) approach for building a high-resolution velocity model. We demonstrate that our method can effectively reconstruct a high-resolution orthorhombic velocity model that fits the geology well and significantly improves the focusing of the fault imaging in a WAZ ocean bottom cable (OBC) dataset. The combined effect of these improvements gives a clear uplift in the final seismic image quality, even when only comparing the impact on the orthorhombic prestack depth migration (PSDM) before and after the FWI update.

Introduction

Orthorhombic anisotropy is considered to be the simplest realistic symmetry for many geophysical problems (Tsvankin, 1997). Orthorhombic anisotropy can be considered as parallel-aligned fractures normally embedded in horizontal thin sedimentary layers; it exhibits both horizontal transverse isotropy (HTI) and vertical transverse isotropy (VTI) effects, making the seismic velocity vary in both azimuthal and polar directions. When the whole fractured bedding system is tilted, it becomes tilted orthorhombic anisotropy, which is a less restrictive assumption and can be applied to more complicated geological formations. In many cases, these effects are important enough to be the target of specialist studies themselves.

The availability of MAZ and WAZ seismic datasets offers the benefit of better illumination in the subsurface. But the presence of orthorhombic anisotropy poses challenges as inconsistent residual moveout due to azimuthal velocity variations are frequently observed in common image gathers (CIGs) from different azimuths. These inconsistent moveouts are often seen in many geologically complex areas, such as fractured thin-bed layers. Being a more general anisotropic model than HTI or VTI, the orthorhombic model can be used to cope with the co-existing HTI/VTI effects in these settings. Thus, orthorhombic PSDM can reduce the structural discrepancies between seismic images built from different azimuths, hence producing a constructive summation of these datasets and also resolving well misties.

Zhou et al. (2015) presented a practical ray-based tomographic inversion flow for orthorhombic model building. However, in geologically complex areas, such as in the presence of complex faults or shallow gas clouds, ray-based tomographic inversion is limited in providing high-resolution velocity models, needed for optimal imaging of complex structures.

FWI is an established velocity model building tool that can generate high-resolution velocity models especially in the areas well probed by diving waves, even in geologically complex areas. However, orthorhombic anisotropy further complicates the already non-linear inversion approach due to an increased number of parameters (Tarantola, 1986; Mora, 1988; Shipp and Singh, 2002; Brossier et al., 2009; Lee et al., 2010; Plessix and Cao, 2011). Therefore, full orthorhombic FWI remains a challenging task.

This paper puts forward a practical FWI approach for high-resolution orthorhombic model building. Our strategy includes a sequential scheme: we first use our tomographic inversion (Zhou et al., 2015) to invert for an orthorhombic model. Then, with this as the starting model, we use orthorhombic FWI to invert for the parameter that impacts the kinematics the most, namely the velocity, while keeping the other orthorhombic parameters fixed.

In the following sections we will describe our orthorhombic FWI approach and illustrate it on a synthetic example. Then we demonstrate with a production OBC WAZ dataset from offshore China how our method can effectively reconstruct the high-resolution orthorhombic model. This model not only fits the geology but also significantly improves the focusing of the fault imaging in the WAZ data.

Orthorhombic full-waveform inversion

The objective of FWI is to minimize the least-squares difference between the predicted and the observed wavefields

$$f = \|Lm - d\|^2 \tag{1}$$

where d is the observed wavefield, L is the modeling operator, and Lm predicts the synthetic wavefield from the model m.

Based on Zhang and Zhang's (2011) formulation, the following second-order wave equation is derived in tilted orthorhombic media with spatially variant density:

$$L\boldsymbol{\sigma} = \frac{1}{V_{p0}^2}\frac{\partial^2 \boldsymbol{\sigma}}{\partial t^2} - \rho N D^T \frac{1}{\rho} D\boldsymbol{\sigma} = s \tag{2}$$

where $\boldsymbol{\sigma} = (\sigma_1, \sigma_2, \sigma_3)^T$ is the vector composing the three principal stresses, s is the source term and

$$N = \begin{bmatrix} 1+2\varepsilon_2 & (1+2\varepsilon_2)\sqrt{1+2\delta_3} & \sqrt{1+2\delta_2} \\ (1+2\varepsilon_2)\sqrt{1+2\delta_3} & 1+2\varepsilon_1 & \sqrt{1+2\delta_1} \\ \sqrt{1+2\delta_2} & \sqrt{1+2\delta_1} & 1 \end{bmatrix} \tag{3}$$

is the parameter matrix for orthorhombic media, and ε_1, ε_2, δ_1, δ_2, δ_3 are the Thomsen parameters for orthorhombic anisotropy (Tsvankin, 1997). Two Euler angles, (ϕ, θ), are used to define the azimuthal and polar angles of the axis tilted from vertical at each spatial point, as for the symmetry axis in a tilted transverse isotropy (TTI) model. For tilted orthorhombic anisotropy, a third angle is introduced to rotate the elastic tensor in the local x-y plane and to represent the orientation of the first crack for an orthorhombic medium composing two orthogonal crack or fracture systems.

$D = diag\left(R_1^T\nabla,\ R_2^T\nabla,\ R_3^T\nabla\right)$ is the tilted first-order derivative and R_i are column vectors of R, the transformation matrix:

$$\begin{pmatrix} \cos\phi & -\sin\phi & 0 \\ \sin\phi & \cos\phi & 0 \\ 0 & 0 & 1 \end{pmatrix}\begin{pmatrix} \cos\theta & 0 & \sin\theta \\ 0 & 1 & 0 \\ -\sin\theta & 0 & \cos\theta \end{pmatrix}\begin{pmatrix} \cos\beta & -\sin\beta & 0 \\ \sin\beta & \cos\beta & 0 \\ 0 & 0 & 1 \end{pmatrix} \tag{4}$$

Finally, V_{p0} is the velocity along the symmetry axis, and ρ is the density, β is the rotation angle in the local plane.

In the adjoint-state method the computation of the gradient of the objective function requires the computation of

$$\left[\frac{\partial L}{\partial m_k}\boldsymbol{\sigma}\right]^T \boldsymbol{\sigma}_b \tag{5}$$

where the right-hand term, $\boldsymbol{\sigma}_b$, is the back-propagated residual wavefield and the left-hand term is constructed from the forward-propagated wavefield and wave equation $L\boldsymbol{\sigma} = s$, where s is the source term. The variable m_k in the partial derivative represents the parameter we would like to update. Hence a V_{p0} update results in

$$\frac{\partial L}{\partial V_{p0}}\boldsymbol{\sigma} = -\frac{2}{V_{p0}^3}\frac{\partial^2 \boldsymbol{\sigma}}{\partial t^2} \tag{6}$$

Orthorhombic FWI for high-resolution model building

The presence of orthorhombic anisotropy makes seismic velocity vary with azimuthal direction. Previously we have put forward a ray-based tomographic inversion flow for orthorhombic model building with WAZ data (Xie et al., 2011, Li et al., 2012; Zhou et al., 2015):

1) Perform TTI tomography using all azimuths together, followed by moveout analysis to see the existence of tilted orthorhombic anisotropy.
2) Apply a TTI tomographic update for each individual azimuth (one TTI model per azimuth).
3) Estimate the fastest velocity direction, angle β, and convert the TTI anisotropy parameters of different azimuths to a set of orthorhombic parameters (V_0, ε_1, δ_1, ε_2, δ_2, δ_3, and β). We inherit (ϕ, θ) from the TTI model.
4) Apply an orthorhombic tomographic velocity update to V_0 and the other orthorhombic anisotropic parameters.

For geologically complex data, such as in the presence of faults or gas clouds, a high-resolution velocity model is desired. We propose to start with the orthorhombic model from the above-mentioned tomographic inversion flow and use our orthorhombic FWI approach to further invert for a high-resolution velocity model, i.e.

5) Apply orthorhombic FWI for a high-resolution velocity model update, adding more details to the velocity model.

Synthetic test

We first demonstrate the validity of our proposed orthorhombic FWI approach using a synthetic dataset. The medium is HTI, with the azimuth angle of the slowest velocity direction (normal to fracture) being 60 degrees from the inline direction in an anti-clockwise manner. Conventionally, HTI is treated as TTI with the polar angle tilted by 90 degrees. HTI is also a special case of orthorhombic anisotropy, with $\varepsilon_1 = \delta_1 = 0$, so it can be represented by an orthorhombic model as well. Hence HTI can be updated by either conventional TTI FWI or our newly developed orthorhombic FWI for V_{p0}. Figure 1 compares the true V_{p0} model, initial V_{p0} model, and the V_{p0} model inverted by conventional TTI FWI and

orthorhombic FWI, respectively. Both conventional TTI and orthorhombic FWI start with the same initial model and a frequency of 3 Hz. Anisotropic parameters are fixed at the true values while only updating V_{p0}. Figure 2 compares the profile at CDP 1800 of the true V_{p0}, initial V_{p0}, V_{p0} by conventional TTI FWI, and V_{p0} by orthorhombic FWI, respectively. The conventional TTI FWI and orthorhombic FWI results agree with each other very well, both becoming closer to the true model in the upper area (0-2 km) that is penetrated by the diving waves. The deeper updates are driven by reflections and, in this example, the poor accuracy of the starting model in, for instance, the central low velocity zone does not allow reflections to correctly update the longer wavelengths of the velocity model. Specific FWI technologies designed to address these problems are needed in these regions (for example, Bi and Lin, 2014).

OBC field data example

The orthorhombic FWI velocity model building flow was applied to a field OBC wide-azimuth 3D seismic dataset. For each patch, eight 6000 m long cables were deployed on the water bottom with 400 m cable separation. The source boat shot along the orthogonal direction with 250 m shot line separation, resulting in a fold coverage of close to 200 with a wide-azimuth distribution.

Figure 3a shows an initial isotropic PSDM CIG in (CDP-offset_y, offset_x) order. The azimuthally dependent variation of the residual moveout clearly shows the presence of azimuthal anisotropy. The orthorhombic tomographic inversion built an initial orthorhombic model and Figure 3b shows the orthorhombic PSDM CIG. By taking into account the co-located VTI and HTI effects, azimuthally dependent residual moveout and non-hyperbolic residual moveout are reconciled. Also, as expected, VTI effects make the vertical velocity lower than the imaging velocity and move events shallower.

To further improve fault imaging, we applied orthorhombic FWI to invert for high-resolution V_{p0}, starting with the velocity model obtained from the above orthorhombic tomographic inversion flow while keeping the anisotropic parameters (ε_1, δ_1, ε_2, δ_2, δ_3) fixed. Figure 4 compares a depth slice of V_{p0} for the initial orthorhombic tomographic model versus the orthorhombic FWI inverted model, both overlaid on the stacked image at 2.1 km. The orthorhombic FWI produces a high-resolution velocity model that is conformal with the faulting structure, as highlighted by the blue arrows. More importantly, in Figure 5 when we look at the stack image and a snail gather from the inline section indicated by the red arrows in Figure 4 (a "snail gather" here is a WAZ CIG ordered into increasing offset with increasing azimuth in each offset band), the orthorhombic FWI model significantly improves the fault imaging. Overall we see much clearer faults with better termination of structures beneath faults and an improved focus in the image caused by the better flattening of events in the CIGs.

Conclusions

The paper demonstrated the effectiveness of a new full-waveform inversion approach for wide-azimuth data imaging in the presence of orthorhombic anisotropy. Synthetic and real data results show that this method can be used to account for both azimuthal and polar direction dependent wave propagation. These elements are of particular importance for MAZ and WAZ surveys where proper treatment of large azimuthal coverage can contribute to a better stack image and give a better tie with the well. Furthermore, our approach produces a high-resolution velocity model that is shown to significantly improve fault imaging.

Acknowledgements

We thank CNOOC for permission to show their data and CGG for permission to publish this work. We also thank Guillaume Thomas-Collignon and Xiaoning Yue for their help. Finally, we thank Chevron/SEG for their 2014 blind test dataset that inspired the synthetic example used here.

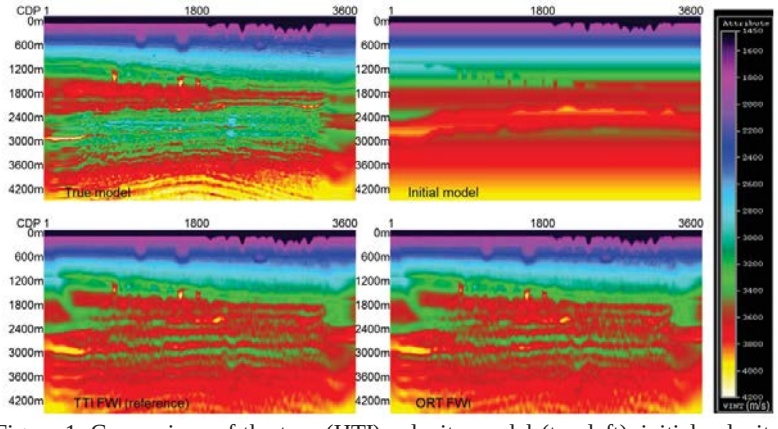

Figure 1: Comparison of the true (HTI) velocity model (top left), initial velocity model (top right), and the velocity model inverted by conventional TTI FWI (running in HTI mode, bottom left) and orthorhombic FWI (also running in HTI mode, bottom right), respectively.

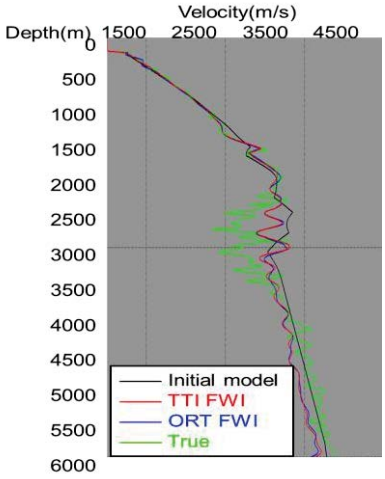

Figure 2: Comparison of velocity profile at CDP 1800, and zoom-in of the comparison.

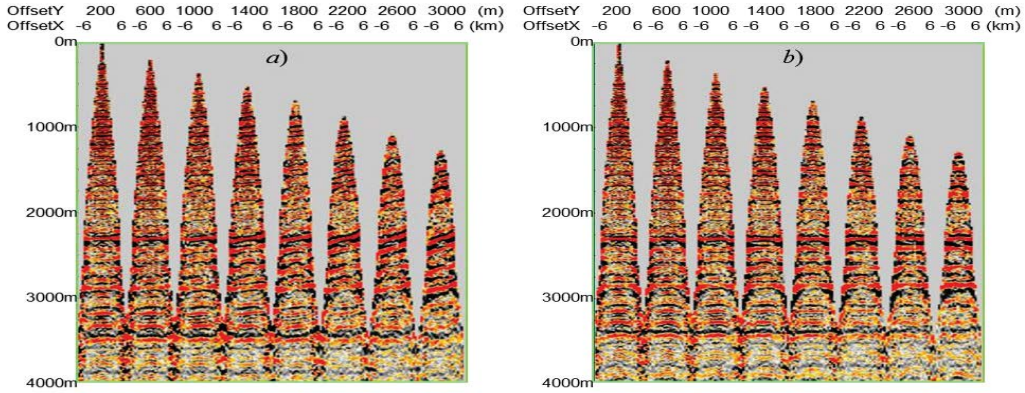

Figure 3: 3D CIGs. a) Isotropic PSDM produces CIG with significant conflicting RMO; b) Orthorhombic PSDM with model from tomographic inversion resolves the conflicting RMO.

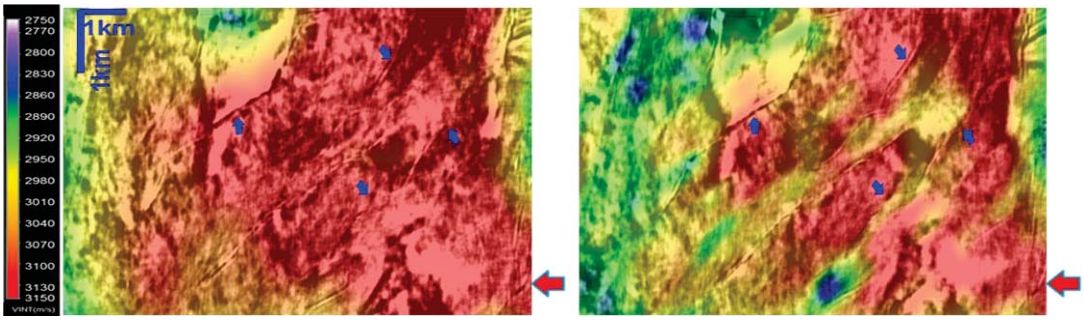

Figure 4: Comparison of V_{p0} depth slice at 2.1 km: a) Model obtained through tomographic inversion; b) Model obtained by orthorhombic FWI; it shows more details and it is more conformal to faulting structures. The red arrow indicates the location of the inline section in Figure 5.

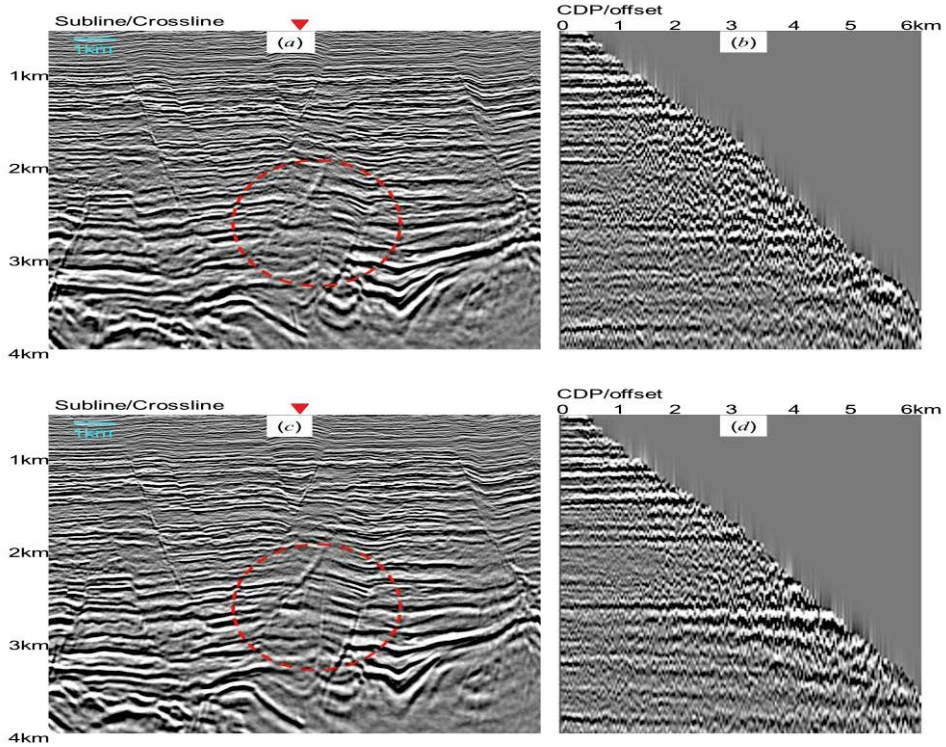

Figure 5: Before and after orthorhombic FWI comparison: a) PSDM stack with original orthorhombic model from tomography, b) PSDM snail gathers with original orthorhombic model from tomography, c) PSDM stack with model after orthorhombic FWI, and d) PSDM snail gather with model after orthorhombic FWI.

EDITED REFERENCES

Note: This reference list is a copyedited version of the reference list submitted by the author. Reference lists for the 2016 SEG Technical Program Expanded Abstracts have been copyedited so that references provided with the online metadata for each paper will achieve a high degree of linking to cited sources that appear on the Web.

REFERENCES

Bi, H., and T. Lin, 2014, Impact of adaptive data selection on full waveform inversion: 84th Annual International Meeting, SEG, Expanded Abstracts, 1094–1098, http://dx.doi.org/10.1190/segam2014-0310.1.

Brossier, R., S. Operto, and J. Virieux, 2009, Seismic imaging of complex onshore structures by 2D elastic frequency-domain full-waveform inversion: Geophysics, **74**, no. 6, WCC105–WCC118, http://dx.doi.org/10.1190/1.3215771.

Lee, H.-Y., J. M. Koo, D.-J. Min, B.-D. Kwon, and H. S. Yoo, 2010, Frequency-domain elastic full waveform inversion for VTI media: Geophysical Journal International, **183**, 884–904, http://dx.doi.org/10.1111/j.1365-246X.2010.04767.x.

Li, Y., W. Han, C. Chen, and T. Huang, 2012, Velocity model building for tilted orthorhombic depth imaging: 82nd Annual International Meeting, SEG, Expanded Abstracts, 1–5, http://dx.doi.org/10.1190/segam2012-1231.1.

Mora, P., 1988, Elastic wave-field inversion of reflection and transmission data: Geophysics, **53**, 750–759, http://dx.doi.org/10.1190/1.1442510.

Plessix, R.-E., and Q. Cao, 2011, A parametrization study for surface seismic full waveform inversion in an acoustic vertical transversely isotropic medium: Geophysical Journal International, **185**, 539–556, http://dx.doi.org/10.1111/j.1365-246X.2011.04957.x.

Shipp, R. M., and S. C. Singh, 2002, Two-dimensional full wavefield inversion of wide-aperture marine seismic streamer data: Geophysical Journal International, **151**, 325–344, http://dx.doi.org/10.1046/j.1365-246X.2002.01645.x.

Tarantola, A., 1986, A strategy for nonlinear elastic inversion of seismic reflection data: Geophysics, **51**, 1893–1903, http://dx.doi.org/10.1190/1.1442046.

Tsvankin, I., 1997, Anisotropic parameters and P-wave velocity for orthorhombic media: Geophysics, **62**, 1292–1309, http://dx.doi.org/10.1190/1.1444231.

Xie, Y., S. Birdus, J. Sun, and C. Notfors, 2011, Multi-azimuth Seismic data imaging in the presence of orthorhombic anisotropy, 73rd Annual International Conference and Exhibition, EAGE, Extended Abstracts, http://dx.doi.org/10.3997/2214-4609.20149223.

Zhang, H., and Y. Zhang, 2011, Reverse time migration in vertical and tilted orthorhombic media: 81st Annual International Meeting, SEG, Expanded Abstracts, 185–189, http://dx.doi.org/10.1190/1.3627568.

Zhou, B., J. Zhou, L. B. Liu, F. C. Loh, J. Liu, Y. Xie, Z. Wang, and X. Pu, 2015, Orthorhombic velocity model building and imaging of Luda field with WAZ OBC data: 85th Annual International Meeting, SEG, Expanded Abstracts, 5212–5216, http://dx.doi.org/10.1190/segam2015-5879535.1.